Phase Transformations in Steelmaking Slags: A Thermodynamic Approach

Tuomas Alatarvas, Rita Kallio, Eetu-Pekka Heikkinen, Qifeng Shu

Process Metallurgy Research Unit, Centre for Advanced Steel Research,
University of Oulu, P.O. Box 4300, FI-90014 Oulu, Finland

Abstract: In addition to solidification, steelmaking slags may undergo phase transformations in solid state during their cooling process. The mineralogy of these oxide slags is significantly influenced by the chemical composition and cooling rate. For the phases forming, two distinct solidification modes can be assumed, depending on the cooling rate: equilibrium cooling and Scheil–Gulliver cooling. Characterization methods, such as scanning electron microscopy (SEM) and electron probe microanalyzer (EPMA) allow analyzing the elemental composition of individual phases. Here, computational thermodynamics were applied in phase identification of crystallized electric arc furnace (EAF) slags. FactSage 8.3 thermodynamic calculation software was used to estimate the composition of stable phases as a function of temperature. Solid solutions with varying compositions were considered in this study. The calculation results from two solidification modes, i.e., equilibrium cooling and Scheil-Gulliver cooling, were saved in Excel spreadsheets. A MATLAB script was developed to go through the results and find the phase with a composition closest to the input values. For both solidification modes, the composition and temperature best fitting the input analysis was determined. The input is the elemental composition of the phase of interest, acquired using EPMA. After the data processing, the results are visualized in graphs, illustrating the analyzed and estimated compositions of the identified solid solution phase and its occurrence temperature.

Keywords: computational thermodynamics, mineralogy, slag, solidification

1. INTRODUCTION

Various types of ferrous slags are generated as by-products of steel industry. During the melting and reduction of iron ore to produce pig iron in a blast furnace, the most voluminous of these, Blast Furnace Slag (BFS) is produced, whereas steel slag is generated either by converting pig iron to steel in a Basic Oxygen Furnace (BOF) or from the melting of scrap to produce steel in Electric Arc Furnace (EAF). According to EUROSLAG data (European Association representing metallurgical slag producers and processors), 37 million tons of slag were produced in 2018, of which 20.7 million tons are BFS and 16.3 million tons are various types of steelmaking slags. EAF slags from carbon steel production represent 26.2% of the steelmaking slags (Euroslag Statistics, 2018). The main applications of steelmaking slags include production of aggregates for road construction, cement or concrete addition, fertilizer, hydraulic engineering, and internal use for metallurgical purposes (Bru et al., 2021).

The physical and chemical characteristics of the EAF slags are dictated by the raw materials used, the constraints of the production process and the cooling method. The main oxide components of EAF slags are iron oxides (FeO_n), lime (CaO), silica (SiO_2), magnesia (MgO) and alumina (Al_2O_3), in addition to minor components such as chromium, manganese and phosphorus oxides (Bru et al., 2021). These components form minerals such as dicalciumsilicates (commonly as monoclinic β form, larnite) monoxide solid solution (Mg,Fe)O, (Mg,Cr,Fe,Al)-spinel, calcium ferrites, calcium aluminates and melilite group members such as gehlenite (Mombelli et al., 2014, Li et al., 2022).

In addition to solidification, steelmaking slags may undergo phase transformations in solid state during their cooling process. The stability of phases in the oxide system can be assessed with computational thermodynamics software such as FactSage (Bale et al. 2002). For a given total composition of the system, the equilibrium composition can be calculated, for instance as a function of temperature. For the phases forming during solidification of molten slags, two distinct solidification modes can be assumed, depending on the cooling rate: equilibrium cooling and Scheil–Gulliver cooling. Equilibrium cooling assumes that the whole system is in equilibrium during the cooling process. On the other hand, the Scheil–Gulliver model, as described by Durinck et al. (2007), assumes no diffusion in the solid phases, infinitely rapid diffusion in the liquid phase, and local equilibrium at the solid/liquid interface. This means that the solidified phases are considered inert, and the final phase structure is reached when the system has completely solidified. Andersson et al. (2024) utilized FactSage for assessing the Scheil–Gulliver solidification sequence of EAF slags with varying composition. The authors reported that for the unmodified slag, with basicity (CaO/SiO_2 ratio) of 2.0, the primary crystallizing phase is monoxide. Modification of the slag by decreasing the basicity to 1.5 and 1.0 promoted the formation of spinel type phases.

The current study presents a method to compare the thermodynamic calculation results with the elemental analysis obtained from steelmaking slags. Interpreting the results

allows the estimation of the formation sequence and temperature for the identified phases.

2. MATERIALS AND METHODS

2.1 Investigated materials

The samples (Slag#1 and Slag#2) provided for this study were produced in two scrap-based EAF steelmaking sites, which manufacture advanced steels for the automotive and engineering industries. Slags are air-cooled with moderate irrigation and processed according to conventional slag-handling procedures including crushing, sieving and magnetic separation stages.

Representative samples from the two sites were delivered to Raahe Research Centre, which conducted the bulk XRF analyses using Malvern Panalytical equipment with Rh X-ray tube and MsDecipher 2.4.17 calculation program. The composition data of the studied slags is presented in Table 1.

Table 1. Chemical composition of the studied slags, in wt.%.

	Slag#1	**Slag#2**
SiO_2	12.13	12.96
Al_2O_3	7.30	8.81
MgO	3.80	8.71
CaO	39.58	32.41
FeO	29.53	30.21
MnO	5.44	4.96
Cr_2O_3	2.22	1.93

2.2 Electron probe microanalyzer

Polished blocks (Ø 25 mm) of the slag samples were prepared for electron probe microanalyzer (EPMA) analysis, which was conducted at the Centre for Material Analysis, University of Oulu. The blocks were coated with carbon prior to analyses. A JEOL JXA-8530FPlus electron probe microanalyzer (JEOL Ltd., Tokyo, Japan) equipped with X-ray Wavelength Dispersive Spectrometer (WDS) was employed to characterize mineral chemical compositions in slags, with the analytical conditions including an accelerating voltage of 15 kV, a beam current of 15 nA, and a beam diameter of 1–10 µm. The peak and background counting times were set at 10 s and 5 s, respectively, for all components. The matrix correction with the ZAF method (atomic number—absorption—fluorescence) was applied. Backscattered electron (BSE) detector was used for imaging of the samples.

2.3 Computational thermodynamics

Computational thermodynamics software FactSage 8.3 and its *FToxid* database were used to estimate the stable phases in the studied materials. In addition to liquid oxide slag, 29 solid solutions from the *FToxid* database were selected for the calculations. Table 2 lists the selected solutions with explanatory composition or mineralogical name. Stoichiometric, pure compounds were not included in the system. For the studied materials, the phase fractions and their compositions were calculated as a function of temperature. In the equilibrium solidification mode, phase stability was calculated in the temperature range of 1800–300 °C. For the Scheil–Gulliver solidification mode, the starting temperature was defined as 1800 °C, where both studied compositions are fully liquid. Here, the cooling step was defined as 25 °C. The results were saved as Excel spreadsheet files.

Table 2. Selected solutions for the calculations.

Solution name	**Example composition or mineralogical name**
A-slag	Liquid oxide slag
B-spinel	Magnetite (Fe_3O_4), Manganoferrite ($MnFe_2O_4$), Manganochromite ($MnCr_2O_4$), Chromite ($FeCr_2O_4$), Galaxite ($MnAl_2O_4$).
A-monoxide	Wüstite (Fe_xO), Lime (CaO), Periclase (MgO), Magnesiowüstite (MgO-Fe_xO), Manganowüstite (Mn-Fe)$_x$O, Manganosite (Mn_xO).
A-Clinopyroxene	Clino-enstatite ($MgSiO_3$), (Metastable) clino-ferrosilite ($FeSiO_3$)
A-Orthopyroxene	Ortho-enstatite ($MgSiO_3$), (Metastable) ortho-ferrosilite ($FeSiO_3$)
A-Protopyroxene	Proto-enstatite ($MgSiO_3$)
LowClinopyroxene	$CaMgSi_2O_6$ - $Mg_2Si_2O_6$ solid solution
A-Wollastonite	$CaSiO_3$
Bredigite	$Ca_3(Ca,Mg)_4Mg(SiO_4)_4$
bC2SA	Ca_2SiO_4
aC2SA	Ca_2SiO_4
A-Melilite	Akermanite ($Ca_2MgSi_2O_7$)
A-Olivine	Forsterite (Mg_2SiO_4), Fayalite (Fe_2SiO_4),
Cordierite	$Al_4Fe_2Si_5O_{18}$ - $Al_4Mg_2Si_5O_{18}$ solution
Mullite	$[Al,Fe]_2[Al,Si,B,Fe][O,Va]_5$
CAFS	$Ca_2(Al,Fe)_8SiO_{16}$
CAF6	$Ca(Al, Fe)_{12}O_{19}$
CAF3	$Ca(Al,Fe)_6O_{10}$
CAF2	$Ca(Al,Fe)_4O_7$
CAF1	$Ca(Al,Fe)_2O_4$
C2AF	$Ca_2(Al,Fe)_2O_5$
C3AF	$Ca_3(Al,Fe)_2O_6$
Corundum	Corundum (Al_2O_3)
Garnets	Grossularite ($Ca_3Al_2Si_3O_{12}$)
CaSpinel	$CaCr_2O_4$ - $CaFe_2O_4$ solid solution
A-Tetragonal-Spinel	Low-temperature Mn_3O_4 dissolving Fe, Mg, Cr, Ti and Al
Bixbyite	Mn_2O_3
Braunite	Non-stoichiometric Mn_7SiO_{12}
Rhodonite	$MnSiO_3$
Pyroxmangite	$MnSiO_3$ - $MgSiO_3$ solution

2.4 Data processing

The procedure for data processing is presented in Fig. 1. The Excel spreadsheet files must be generated once for a sample

with a specified composition. After that, the phase identification is carried out using MATLAB scripting. As input values, the WDS point analysis of Mg, Al, Si, Ca, Cr, Mn, and Fe is compared with the compositions of all existing phases at all temperatures, read from the Excel spreadsheets.

The results are then visualized for a given point analysis, showing the best R^2 fit for the calculated vs. analyzed Mg, Al, Si, Ca, Cr, Mn, and Fe contents, along with their occurrence temperature for both equilibrium cooling and Scheil–Gulliver solidification modes.

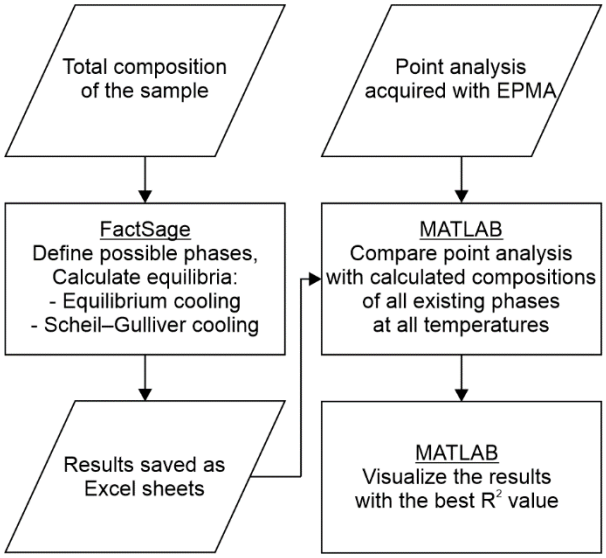

Fig. 1. Flowsheet for the data processing.

3. RESULTS AND DISCUSSION

3.1 Slag#1

The fractions of equilibrated phases according to equilibrium cooling in Slag#1 is presented in Fig. 2. At 1800 °C, the slag is fully liquid. As the temperature decreases to approx. 1700 °C (liquidus temperature), tetragonal spinel is the first solid phase to form, followed by monoxide phase at around 1500 °C. As the temperature further decreases to 1050 °C, the system is completely solid (solidus temperature). The results reveal solid state phase transformations of silicate phases bC2SA, bredigite and olivine. In addition, stable phases include calcium aluminate C3AF with Fe solubility, another monoxide phase, and a small amount of another spinel phase (B-spinel) below 400 °C.

Scheil–Gulliver solidification results for Slag#1 are presented in Fig. 3. Tetragonal spinel is the first forming solid phase, followed by monoxide. Other phases to form during solidification are bC2SA and C3AF. In this case, the solidus temperature is comparable to the value with equilibrium cooling. By definition, solid state transformations do not occur in Scheil–Gulliver solidification. Therefore, bC2SA silicate exists in the final solidification phase structure.

BSE image of Slag#1 sample is presented in Fig. 4, acquired with EPMA. The phase identification procedure results are presented for selected points of interest: A, B, and C with distinct grayscale brightness.

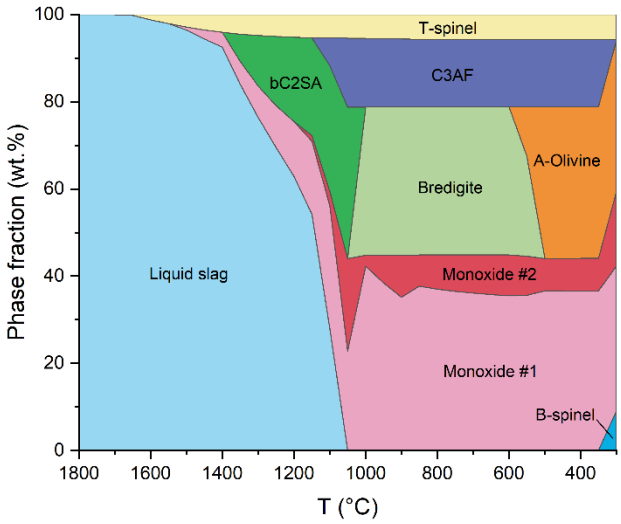

Fig. 2. Phase fractions in Slag#1, equilibrium cooling.

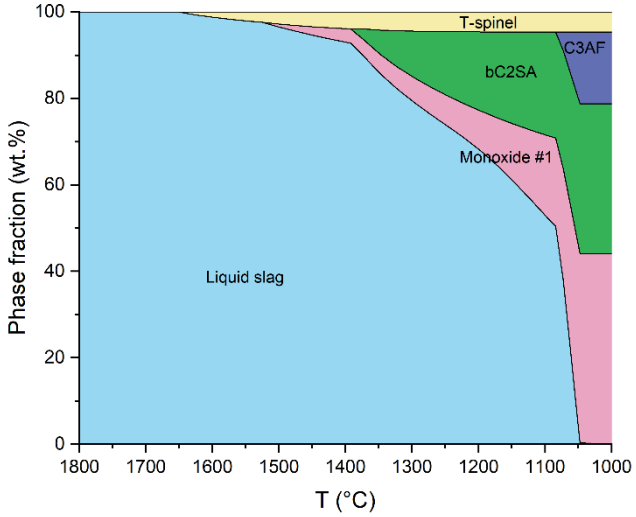

Fig. 3. Phase fractions in Slag#1, Scheil–Gulliver solidification.

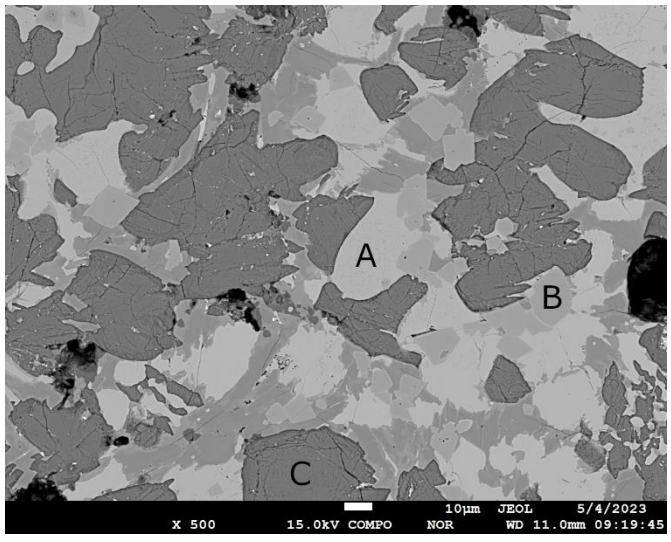

Fig. 4. BSE image of Slag#1.

The graphs presented in Fig. 5 present the WDS analyzed contents of Mg, Al, Si, Ca, Cr, Mn, and Fe for point A in Fig. 4. Comparing to the FactSage calculated values, it is found that the analyzed values correspond best to monoxide phase around 1100–1150 °C both for equilibrium cooling and Scheil–Gulliver solidification. According to the chemical composition, this appears to be a wüstite based solid solution (Fe,Mn,Mg,Cr)O.

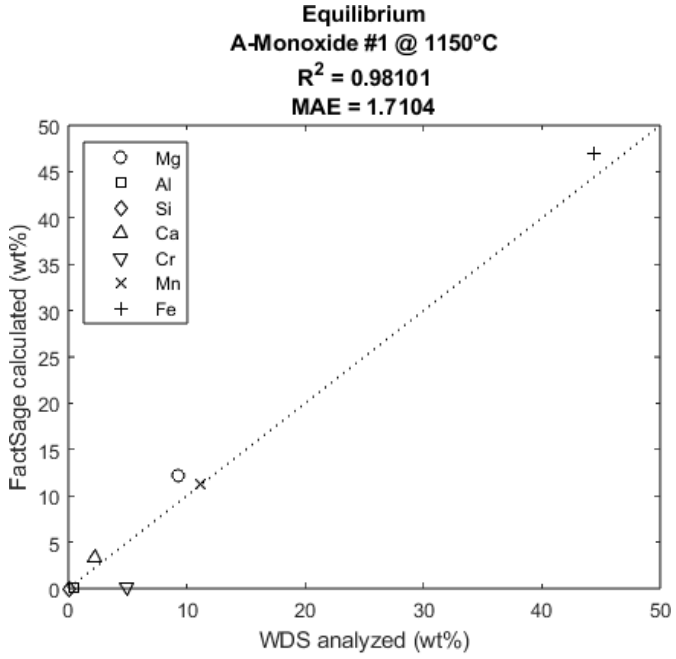

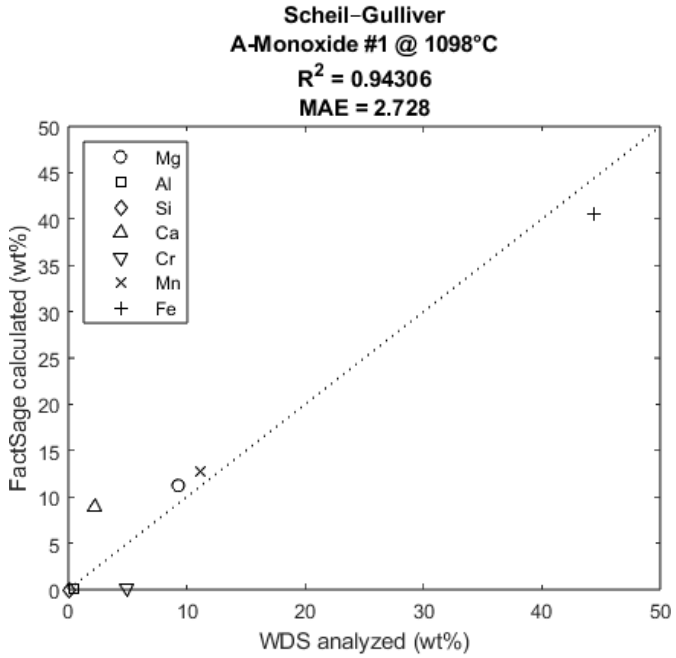

Fig. 5. Elemental composition of point A compared to the calculated stable phases in Slag#1.

For point B observed in Fig. 4, the results are shown in Fig. 6. According to both cooling calculations, the composition is closest to tetragonal spinel occurring at high temperatures, with an R^2 value of approx. 0.63. Noting the analyzed high chromium content, the phase composition is close to chromite ($FeCr_2O_4$), another spinel phase.

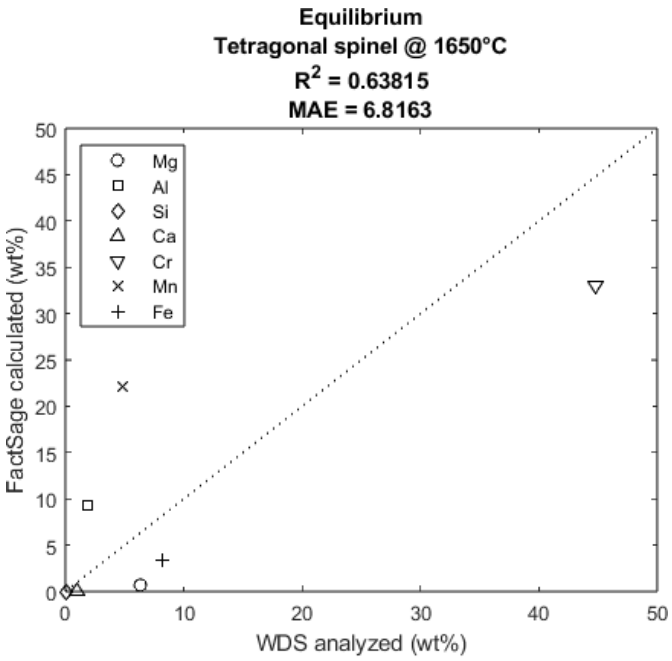

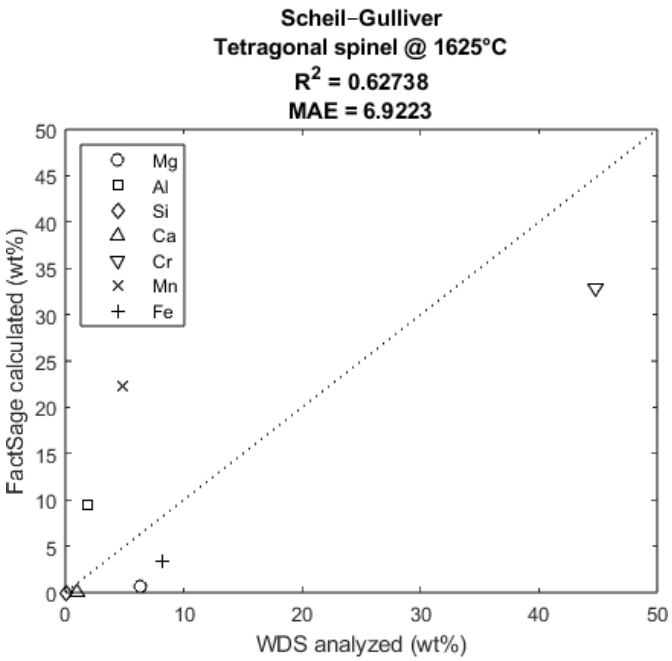

Fig. 6. Elemental composition of point B compared to the calculated stable phases in Slag#1.

It is observed in Fig. 7 that the composition in point C contains mostly calcium and silicon, whereas other considered elements are close to zero, suggesting a silicate phase. The equilibrium cooling calculation indicates that the phase is olivine at the minimum calculation temperature. The Scheil–Gulliver solidification calculation shows another silicate phase, bC2SA.

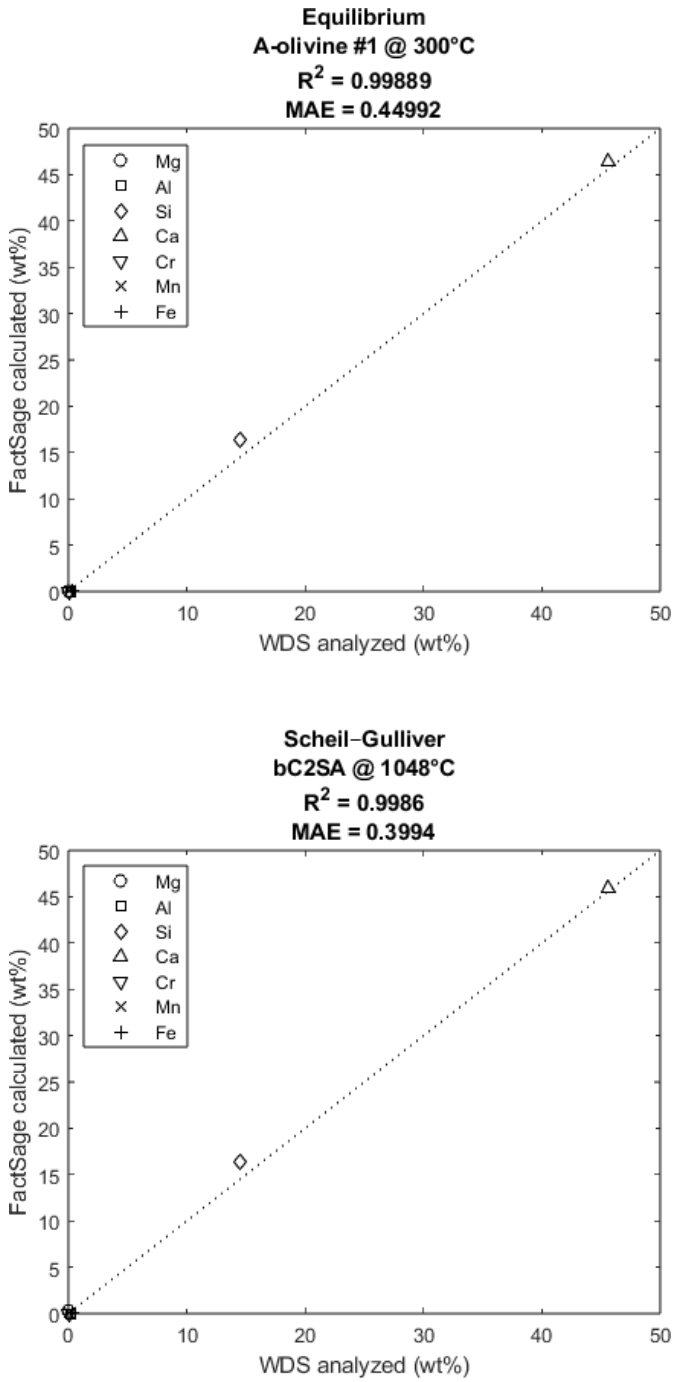

Fig. 7. Elemental composition of point C compared to the calculated stable phases in Slag#1.

3.2 Slag#2

The fractions of phases according to equilibrium cooling in Slag#2 is presented in Fig. 8. At 1800 °C, the slag is fully liquid. As the temperature decreases to approx. 1700 °C, monoxide is the first solid phase to form, followed by tetragonal spinel almost immediately. The system is completely solid at ~1100 °C. Similarly to Slag#1, silicate phases bC2SA, bredigite and olivine undergo solid state phase transformation. A stability region of calcium aluminates CAF1 and C3AF is found, both with Fe solubility. Another monoxide phase and B-spinel appear at relatively low temperatures.

The Scheil–Gulliver solidification results for Slag#2 are presented in Fig. 9. As expected from the equilibrium cooling results, the first forming solid phases are monoxide and tetragonal spinel. Other precipitating phases include bC2SA, CAF1, and C3AF. Contrary to equilibrium cooling, melilite phase exists in the results. Here, the solidus temperature is lower (~1050 °C) than in equilibrium cooling (~1100 °C).

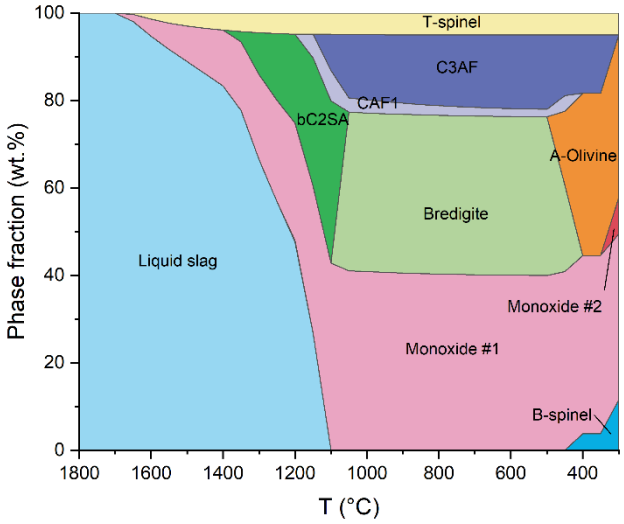

Fig. 8. Phase fractions in Slag#2, equilibrium cooling.

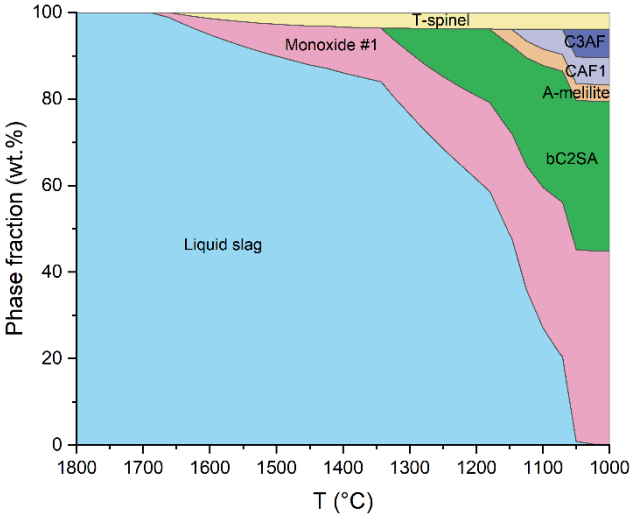

Fig. 9. Phase fractions in Slag#2, Scheil–Gulliver solidification.

BSE image of Slag#2 sample is presented in Fig. 10. For the second slag sample, the procedure results are presented for selected points of interest: D, E, and F.

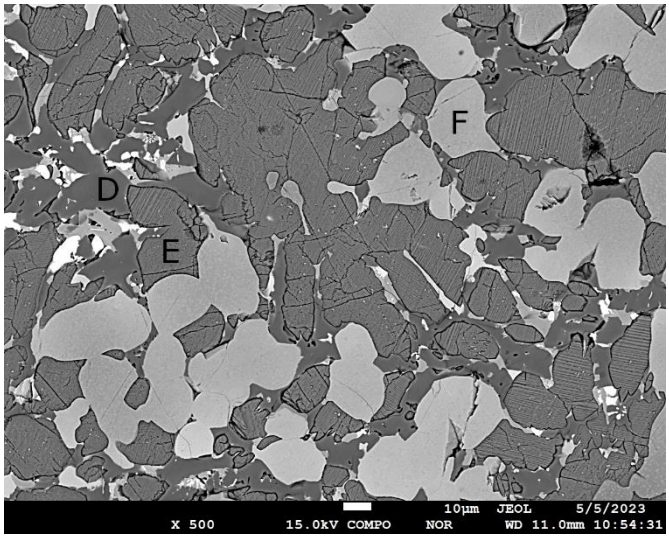

Fig. 10. BSE image of Slag#2.

For point D, the phase identification results are plotted on Fig. 11. Here, the WDS analysis contains mostly calcium and aluminum, with near-zero amount of other considered elements. From both calculation results, the composition corresponds to calcium aluminate C3AF. The calculated composition is very close to stoichiometric $3CaO{\cdot}Al_2O_3$ in both cases, explaining the identical resulting R^2 values.

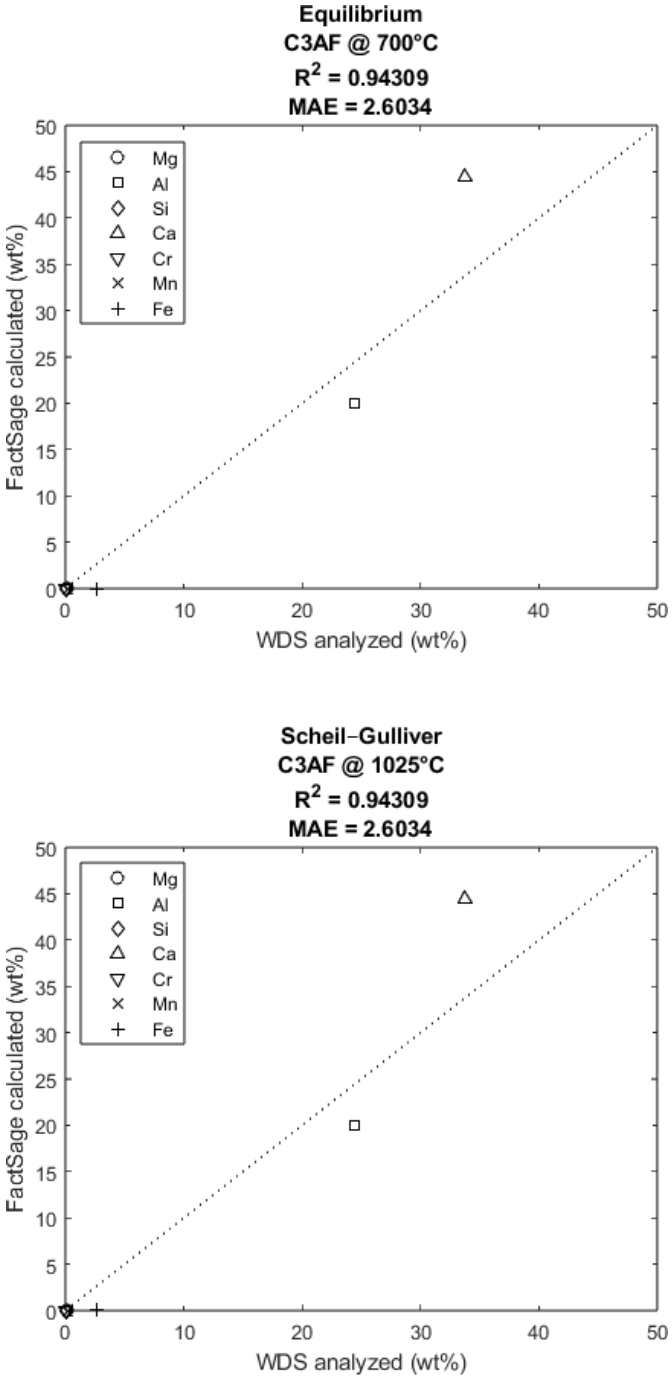

Fig. 11. Elemental composition of point D compared to the calculated stable phases in Slag#2.

It is observed in Fig. 12 that the composition in point E contains mostly calcium and silicon, whereas other considered elements are close to zero, suggesting a silicate phase. The equilibrium cooling calculation indicates that the phase is olivine occurring at low temperatures. The Scheil–Gulliver solidification calculation shows another silicate phase, bC2SA with a composition occurring at 1025 °C.

Figure 13 shows the results for point F in Slag#2. Comparing to the calculated values, it is observed that the analyzed values match a monoxide phase both for equilibrium cooling and Scheil–Gulliver solidification. According to the WDS analysis, this appears to be a wüstite based solid solution (Fe,Mn,Mg,Cr)O.

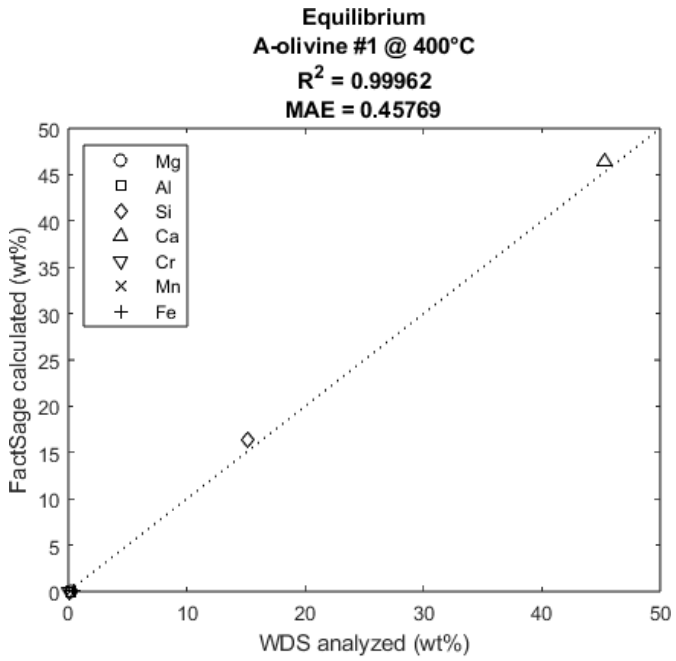

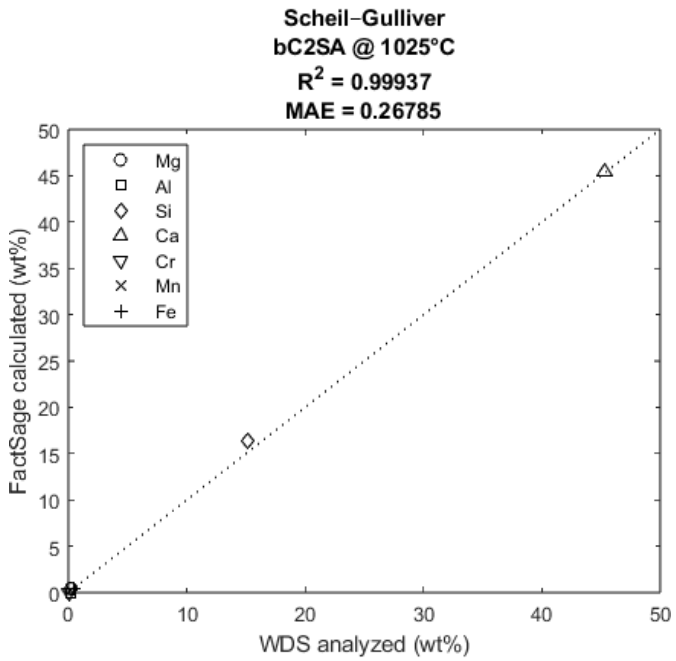

Fig. 12. Elemental composition of point E compared to the calculated stable phases in Slag#2.

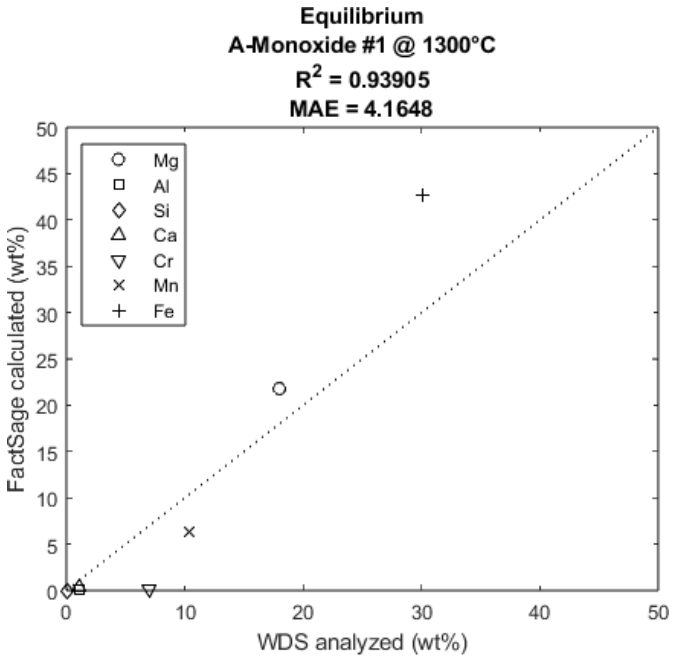

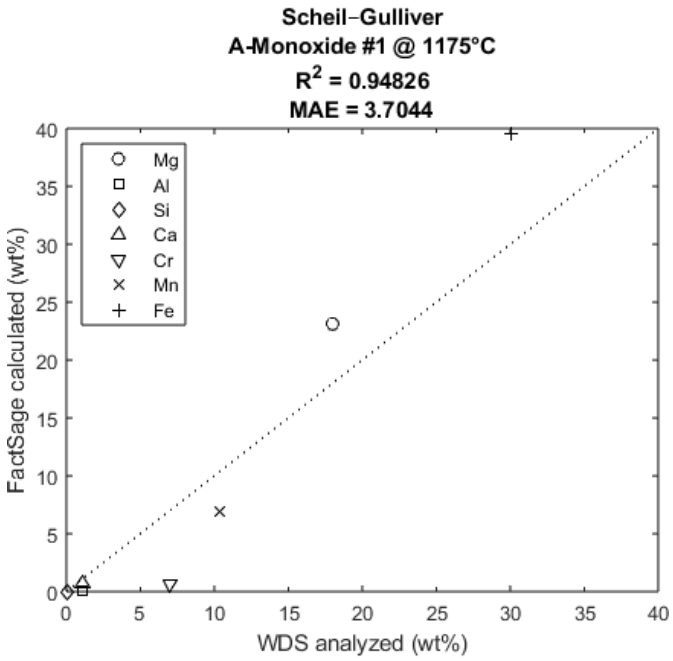

Fig. 13. Elemental composition of point F compared to the calculated stable phases in Slag#2.

4. CONCLUSIONS

In addition to chemical composition, the cooling rate affects the phases forming during solidification and cooling of oxide-based steelmaking slags. The thermodynamic calculation software FactSage was used to estimate the phase fractions and their composition as a function of temperature, according to equilibrium cooling and Scheil–Gulliver solidification. The current study presents a method to compare the thermodynamic calculation results with the elemental analysis obtained from steelmaking slags. Interpreting the results allows the estimation of the formation sequence and temperature for the identified phases.

In this study, two EAF slag materials, samples Slag#1 and Slag#2 were investigated. The thermodynamic calculations show some similarities in the materials: the stable phases include monoxide (wüstite), spinel, calcium silicates and calcium aluminate phases. The equilibrium cooling results illustrated solid state phase transformations of calcium silicates, bC2SA–bredigite–olivine with decreasing temperature. The presented phase identification procedure can be used to visualize the elemental composition of the analyzed points and confirm the mineralogical group. For monoxide phases, calcium silicates, and calcium aluminates, the FactSage calculated and WDS analyzed compositions correspond with excellent R^2 values (>0.9). However, the FactSage calculated chromium content in spinel phase (chromite $FeCr_2O_4$), was lower than analyzed, resulting in moderate R^2 value.

The presented approach can be used to visualize the results for different experimental scenarios: altering the cooling rate of the slag, effect of iron saturation in the system, or the atmosphere effect. In addition, the results using different databases in the FactSage calculations can be compared.

The procedure is not restricted to slag materials, instead, a similar approach can be applied to other systems where solidification and possible solid state phase transformations take place. Besides EPMA, other analysis methods can be employed, for instance Scanning Electron Microscope (SEM).

ACKNOWLEDGEMENTS

The authors are grateful to the funding of the research program FFS2 (Towards Fossil-Free Steel 2, 5534/31/2023) funded by Business Finland.

REFERENCES

Andersson, A., Isaksson, J., Lennartson, A., and Engström, F. (2024). Insights into the Valorization of Electric Arc Furnace Slags as Supplementary Cementitious Materials. *Journal of Sustainable Metallurgy* 10(1), 96– 109.

Bale, C.W., Chartrand, P., Degterov, S.A., Eriksson, G., Hack, K., Mahfoud, R.B., Melançon, J., Pelton, A.D., and Petersen, S. (2002), FactSage Thermochemical Software and Databases. *Calphad* 26(2), 189–228.

Bru, K., Seron, A., Morillon, A., Algermissen, D., Lerouge, C. and Menad, N. (2021). Characterization of a Chromium-Bearing Carbon Steel Electric Arc Furnace Slag after Magnetic Separation to Determine the Potential for Iron and Chromium Recovery. *Minerals*, 12(1), 47.

Durinck, D., Jones, P.T., Blanpain, B., and Wollants, P. (2007). Slag Solidification Modeling Using the Scheil–Gulliver Assumptions. *Journal of the American Ceramic Society,* 90 (4), 1177–1185.

Euroslag. Statistics (2018). Available online: https://www.euroslag.com/products/statistics/statistics-2018/ (accessed on 8 May 2024).

Li, Y., Guo, K., Xiang, J., Pei, G., Lv, X. (2022). Effect of cooling method on the mineralogy and stability of steel slag. *ISIJ International*, 62 (11), 2197–2206.

Mombelli, D., Mapelli, C., Barella, S., Di Cecca, C., Le Saout, G. and Garcia-Diaz, E. (2016). The effect of chemical composition on the leaching behaviour of electric arc furnace (EAF) carbon steel slag during a standard leaching test. *Journal of Environmental Chemical Engineering* 4(1), 1050–1060.